

3C 294 revisited: Deep Large Binocular Telescope AO NIR images and optical spectroscopy[★]

J. Heidt¹, A. Quirrenbach¹, N. Hoyer¹, D. Thompson², A. Pramskiy¹, G. Agapito³, S. Esposito³, R. Gredel⁴, D. Miller², E. Pinna³, A. Puglisi³, F. Rossi³, W. Seifert¹, and G. Taylor³

¹ Landessternwarte, Zentrum für Astronomie der Universität Heidelberg, Königstuhl 12, 69117 Heidelberg, Germany
e-mail: jheidt@lsw.uni-heidelberg.de

² LBT Observatory, University of Arizona, 933 N. Cherry Ave, Tucson, USA

³ Arcetri Astrophysical Observatory, Largo E. Fermi 5, 50125 Firenze, Italy

⁴ Max-Planck-Institut für Astronomie, Königstuhl 17, 69117 Heidelberg, Germany

Received NN; accepted NN

ABSTRACT

Context. High redshift radio galaxies are among the most massive galaxies at their redshift, are often found at the center of protoclusters of galaxies, and are expected to evolve into the present day massive central cluster galaxies. Thus they are a useful tool to explore structure formation in the young Universe.

Aims. 3C 294 is a powerful FR II type radio galaxy at $z = 1.786$. Past studies have identified a clumpy structure, possibly indicative of a merging system, as well as tentative evidence that 3C 294 hosts a dual active galactic nucleus (AGN). Due to its proximity to a bright star, it has been subject to various adaptive optics imaging studies.

Methods. In order to distinguish between the various scenarios for 3C 294, we performed deep, high-resolution adaptive optics near-infrared imaging and optical spectroscopy of 3C 294 with the Large Binocular Telescope.

Results. We resolve the 3C 294 system into three distinct components separated by a few tenths of an arcsecond on our images. One is compact, the other two are extended, and all appear to be non-stellar. The nature of each component is unclear. The two extended components could be a galaxy with an internal absorption feature, a galaxy merger, or two galaxies at different redshifts. We can now uniquely associate the radio source of 3C 294 with one of the extended components. Based on our spectroscopy, we determined a redshift of $z = 1.784 \pm 0.001$, which is similar to the one previously cited. In addition we found a previously unreported emission line at $\lambda 6749.4 \text{ \AA}$ in our spectra. It is not clear that it originates from 3C 294. It could be the Ne [IV] doublet $\lambda 2424/2426 \text{ \AA}$ at $z = 1.783$, or belong to the compact component at a redshift of $z \sim 4.56$. We thus cannot unambiguously determine whether 3C 294 hosts a dual AGN or a projected pair of AGNs.

Key words. Instrumentation: adaptive optics – Galaxies: active – Galaxies: high-redshift – (Galaxies:) quasars: emission lines – (Galaxies:) quasars: individual: 3C 294

1. Introduction

Within the standard unified scheme for active galactic nuclei (AGN), radio galaxies are seen at relatively large inclination angles between the observer and the jet axis (Urry & Padovani 1995). Since most of the optical emission from the central engine is shielded by the dusty torus, they can be used to study their host galaxies and immediate environment in better detail than their low-inclination counterparts. This is particularly important for powerful radio galaxies at high redshifts, which are among the most massive galaxies at their redshift (Overzier et al. 2009). They are expected to evolve to present day massive central cluster galaxies and are often found at the center of (proto)clusters (see Miley & De Breuck (2008) for a review). Recently, even a radio galaxy at $z = 5.72$ close to the presumed end of the epoch of

reionization has been found by Saxena et al. (2018). Thus studies of these species allow us to investigate the early formation of massive structures in the young Universe.

3C 294 is a powerful Fanaroff-Riley type II (FR II) radio source at $z = 1.786$. It shows a z-shaped morphology at $\lambda 6 \text{ cm}$, has extended Ly α -emission, which is roughly aligned with the radio jet axis (McCarthy et al. 1990), is embedded in extended diffuse X-ray emission indicative of a high-density plasma region (Fabian et al. 2003), and is surrounded by an apparent overdensity of faint red galaxies (Toft et al. 2003).

Due to its proximity to a bright star useful for adaptive optics (AO) imaging, 3C 294 has been intensively studied using the Keck, Subaru, and Canada France Hawaii (CFHT) telescopes. High-resolution H and K images of the 3C 294 system have been presented and discussed by Stockton et al. (1999), Quirrenbach et al. (2001), and Steinbring et al. (2002). There is common agreement across all studies that the 3C 294 morphology can best be described by two or three components separated by $\leq 1''$, indicative of a merging system. It is unclear, however, which of the components coincides with the location of the radio source, mostly due to the uncertain position of the reference star used for the astrometry. In addition, some of the components are

[★] The LBT is an international collaboration among institutions in the United States, Italy, and Germany. LBT Corporation partners are: The University of Arizona on behalf of the Arizona Board of Regents; Istituto Nazionale di Astrofisica, Italy; LBT Beteiligungsgesellschaft, Germany, representing the Max-Planck Society, The Leibniz Institute for Astrophysics Potsdam, and Heidelberg University; The Ohio State University, and The Research Corporation, on behalf of The University of Notre Dame, University of Minnesota, and University of Virginia.

compact, others extended, adding more uncertainty to a unique assignment of the counterpart to the radio source. The situation became even more complex after an analysis of archival Chandra data of 3C 294 by Stockton et al. (2004), who found the central X-ray emission to be better represented by two point sources. They argued that 3C 294 hosts a dual AGN, one unabsorbed system associated with a compact component and one absorbed system associated with one of the extended components.

Small separation (a few kiloparsec) bound dual AGN are predicted to be rare in general (see Rosas-Guevara et al. (2019)). On the other hand, as discussed in Koss et al. (2012), the percentage of dual AGN can be up to 10%, but they are difficult to detect in particular at high redshift due to their small projected separation. In fact, only a few high-redshift ($z > 0.5$) dual AGN are known (Husemann et al. 2018, and references therein). If 3C 294 were to evolve to a present day massive central cluster galaxy, one would assume that its mass would grow mostly via major mergers in the hierarchical Universe. Since supermassive black holes seems to reside at the centers of all massive galaxies (Kormendy & Ho 2013), one could expect that 3C 294 hosts a dual AGN. Thus a confirmation would be an important detection.

To unambiguously determine the properties of the 3C 294 system and in particular to test whether it is a dual AGN or an AGN pair, we carried out high-resolution adaptive optics (AO) supported imaging in the near-infrared (NIR) zJHKs bands, as well as deep optical low-resolution spectroscopy using the Large Binocular Telescope (LBT), the results of which are presented here. We note that the AO data discussed above were taken about 15 years ago. Since then adaptive optics AO systems and NIR detectors have become much more mature and efficient. The only spectroscopic investigation of 3C 294, by McCarthy et al. (1990), dates back more than 25 years and was carried out using the Shane 3 m reflector. Thus a revisiting of the 3C 294 system should give a clear answer.

Throughout the paper, we assume a flat Λ CDM cosmology with $H_0 = 70$ km/s/Mpc and $\Omega_M = 0.3$. Using this cosmology, the angular scale is 8.45 kpc per arcsecond at $z = 1.786$.

2. Observations and data reduction

2.1. NIR AO imaging data

High-resolution FLAO (first light adaptive optics, Esposito et al. (2012)) supported data of 3C 294 were recorded in the zJHKs filters with the NIR imager and spectrographs LUCI1 and LUCI2 at PA = 135° during a commissioning run on March 20, 2016 and during a regular science run on March 20, 25, and 29, 2017. In both LUCI instruments, we used the N30-camera, which is optimized for AO observations. With a scale of $0.0150 \pm 0.0002''/\text{pixel}$, the field of view (FoV) offered was $30'' \times 30''$. The observing conditions were very good during all of the nights, with clear skies and ambient seeing of 1'' or less.

The LUCI instruments are attached to the front bent Gregorian focal stations of the LBT. The LBT offers a wide range of instruments and observing modes. It can be operated in monocular mode (using one instrument and mirror only), binocular mode (using identical instruments on both mirrors), or interferometric mode (light from both telescopes combined in phase). A complete description of the current instrument suite at the LBT and its operating mode can be found in Rothberg et al. (2018). The data obtained on March 20, 2016 and March 20 and 25, 2017 were taken in monocular mode, while the data from March 29, 2017 were taken in binocular mode. For the latter, the integrations and offsets were done strictly in parallel.

The FLAO system senses the atmospheric turbulence by means of a pyramid-based wavefront sensor, which samples the pupil on a grid of 30×30 subapertures. A corrected wavefront is obtained through an adaptive secondary mirror controlled by 672 actuators at a frequency of up to 1 kHz. As a reference star we used the 12th mag star U1200-07227692 from the United States Naval Observatory (USNO) catalog USNO-A2.0 (Monet 1998), which is just 10'' southwest of 3C 294. Given its brightness, the FLAO system corrected 153 modes with a frequency of 625 Hz. At this distance of the target from the reference star and with this FLAO configuration, a Strehl ratio of about 30-40% is expected in H and Ks bands (Heidt et al. 2018). U1200-07227692 is a binary star with 0.135'' separation and a brightness ratio of 1:1.6 (Quirrenbach et al. 2001), but this did not affect the performance of the FLAO system.

Individual LUCI exposures were one minute each, consisting of six images of 10 sec that were summed before saving. On any given night, integrations between 7 and 37 min in total were taken in one filter before moving to the next. Table 1 gives a log of the observations. Between each one-minute exposure the telescope was shifted randomly within a $2'' \times 2''$ box to compensate for bad pixels. Since the bright reference star is the only object in the field present in one-minute integrations, larger offsets would not have made any difference as the detector is particularly prone to persistence. The small offsets made sure that none of the images of 3C 294 fell on a region on the detector affected by persistence from the bright reference star. In Table 2 a breakdown of the total integration times by filter and instrument is given.

Date	Instrument	Filter	N_{images}	T_{int} [sec]
Mar 20 2016	LUCI1	Ks	22	1320
		H	7	420
Mar 20 2017	LUCI2	Ks	37	2220
		z	31	1860
Mar 25 2017	LUCI1	J	30	1800
		Ks	32	1920
		J	15	900
		H	30	1800
Mar 29 2017	LUCI1	Ks	19	1140
		J	15	900
	LUCI2	H	30	1800
		Ks	20	1200

Table 1. Breakdown of the observations by date, instrument, and filter.

Filter	LUCI1 [s]	LUCI2 [s]	T_{total} [s]
z	1860	-	1860
J	2700	900	3600
H	1800	2220	4020
Ks	4380	3420	7800

Table 2. Total integration times per filter and instrument and for both instruments combined. Combined exposure times range from 31 minutes to over 2 hours.

The data were first corrected for non-linearity using the prescription given in the LUCI user manual, then sky-subtracted and flat-fielded. Sky-subtraction was achieved by forming a median-combined two-dimensional sky image out of all data in one filter set, then subtracting a scaled version from each individual exposure. Given the fine sampling of $0''.015/\text{pixel}$ scale, we saw

only about 10 counts/sec in the H and Ks bands. With such low backgrounds there would have been no benefit in using a running mean or a boxcar for the sky subtraction. Flatfields were created out of sets of higher and lower background twilight images taken at zenith, which were separately median-combined after scaling them, subtracted from each other, and normalized. Finally, the images were corrected for bad pixels by linear interpolation. A bad pixel mask was created out of the highly exposed flatfields to identify cold pixels and dark images to identify hot pixels.

The most difficult part of the data reduction was the stacking of the images. Except for the saturated AO reference star and the barely visible radio galaxy, no further objects are present on the reduced images that could be used for the alignment of the images. We thus explored three alternative possibilities for the alignment: a) to use the world coordinate system (WCS) information given in the image headers; b) to use a two-dimensional fit to the centers of both saturated components of the reference star after masking the saturated pixel at their centers; and c) to take advantage of the channel crosstalk shown by the detector, which leaves a non-saturated imprint of the reference star in every channel of the detector on the frame (see Fig. 1).

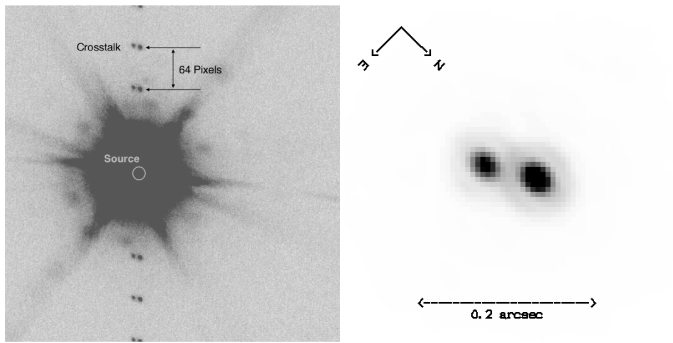


Fig. 1. Left) Image and channel crosstalk images of the reference star U1200-07227692. The center of the reference star is indicated as source. These crosstalk images have separations of exactly 64 pixels, the width of each of the 32 parallel amplifier channels of the LUCI HAWAII2-RG detector. The well-separated images of the individual components of the reference star are remarkable. Right) Logarithmic image of the center of the reference star to show the two components separated by $0.135''$. The Ks-band image is taken at PA = 135° .

The simple approach using the WCS information failed, likely because of residual flexure within LUCI, resulting in a visibly "smeared" image of the reference star. We thus did not pursue this approach further. Each of the two alternative methods has its advantages and disadvantages. Determining a centroid of a saturated core leaves some uncertainty but it benefits from a high signal-to-noise ratio (S/N) in its outer parts. The individual channel crosstalk images have a lower S/N, but combining 10-15 of them from adjacent channels increases the signal considerably. We tested both methods using a data set taken in the Ks filter. The resulting offsets agree within 1/10 of a pixel. Given that we opted for integer pixel shift before combining the images, both methods delivered equally good results for our purposes. In the end we decided to use the offsets derived from the centroids to the cores of the two components of the reference star.

The aligned images were first combined per filter, instrument, and night, then per filter and telescope, and finally per filter. The relative orientation of the detector on the sky between the two instruments differs by less than one degree. In addition, the pixel scale between the N30 cameras in LUCI1 and LUCI2

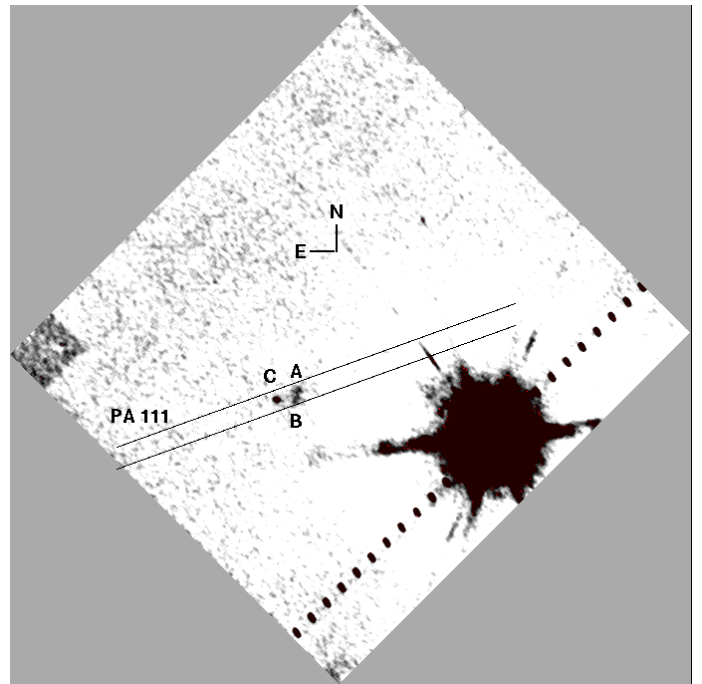


Fig. 2. Orientation of the slit with respect to the 3C 294 system for the MODS spectroscopy.

differs by less than 10^{-4} . Thus no rotation or rebinning was applied before combining the data sets from the different instruments.

2.2. Optical spectroscopy

Optical longslit spectra of the 3C 294 system were taken on the night of May 11-12, 2016 using the multi-object double CCD spectrographs MODS1 and MODS2 (Pogge et al. 2010) in homogeneous binocular mode. The MODS instruments are attached to the direct Gregorian foci at the LBT. The target was observed at PA = 111° in order a) to have all components of the 3C 294 system in the slit, b) to see whether components a, b, and c are at the same redshift, and c) to minimize the impact of the nearby bright star on the data quality (see Fig. 2 for the configuration of MODS1/2 and Fig. 3 for more details on the components). To do so, we performed a blind offset from the bright reference star, with the offset determined from the AO K-band image. The expected accuracy of the positioning is $\sim 0.1''$. We used a 1" slit and the gratings G400L for the blue and G670L for the red channel, giving a spectral resolution of about 1000 across the entire optical band. Integration times were 3×1200 sec. Observing conditions were not photometric with variable cirrus, but excellent seeing ($\sim 0.7''$ full width at half maximum (FWHM)).

The basic data reduction (bias subtraction and flatfielding) was carried out using the modsCCDRED-package developed by the MODS team (Pogge 2019). The extraction of one-dimensional spectra was carried out using the standard image reduction and analysis facility (IRAF) *apall* task. As the spectra of 3C 294 did not show any continuum (Fig. 4) and were taken through variable cirrus, we did not carry out a spectrophotometric flux calibration. Wavelength calibration was done using spectral images from calibration lamps and verified using the night sky emission lines. The resulting accuracy was $\sim 0.1 \text{ \AA}$ rms. The resulting spectra were first averaged per telescope and channel and then combined per channel.

3. Results

3.1. AO NIR images of 3C 294

The final AO J-, H-, and Ks-band images are shown in the lower part of Fig. 3. They have been binned by a factor of two to emphasize structures more clearly.

As discussed in Quirrenbach et al. (2001) and Steinbring et al. (2002), 3C 294 can be separated into two main components separated by about $1''$: a compact core-like structure to the east and a structure elongated north–south to the west. The elongated structure seems to consist of two knotty components also separated by roughly $1''$. No emission from 3C 294 was detected in the z-band image. This is probably due to the shallow depth of the image, the much lower Strehl ratio, and/or the increasing extinction compared to the redder bands. We note that 3C 294 has only barely been detected in optical broadband images with the Hubble Space Telescope (HST) ($m_R = 23.4 \pm 0.8$, Steinbring et al. (2002)).

Contrary to earlier observations, the two components of the western component are clearly separated. A comparison of earlier H- and K-band images with our data is shown in Fig. 3.

We do not see a clear separation of the western structures in the J band. The reason for that is not clear. It cannot be due to extinction by dust as the H and Ks bands would be less affected by that (Ks band probes the rest-frame wavelength at $\sim 7700 \text{ \AA}$ and J band probes the rest-frame wavelength at $\sim 4400 \text{ \AA}$). It is more likely due to the lower Strehl ratio, which is expected to drop by 10–20% between the H band and the J band. We do not detect the component d north of component c discussed in Steinbring et al. (2002) in any of our images. We should have detected it in the H band as both components have a similar brightness in this filter according to Steinbring et al. (2002). Thus, feature d is either a transient phenomenon or is not physical, that is, it is a statistical noise fluctuation. There may, however, be some (very blue?) emission northwest of component c in the J-band image, which is not at the same location as component d.

The core-like component c appears slightly extended in an east–west direction on the images. This can also be seen in data from other telescopes shown in Fig. 3. Its measured FWHM is $0''.31 \times 0''.20$ in the H band and $0''.23 \times 0''.17$ in the Ks band. If component c were a pure point source, we would expect a FWHM of about $0''.08$ at $10''$ from a 12th mag reference star (Heidt et al. 2018). Interestingly, the major axis of the elongation is perpendicular to the one seen for the reference star in Fig. 1. The latter is most likely due to vibrations of the telescope (D. Miller, priv. com.) and present on some of the individual images. The former could be due to tilt anisoplanatism as it is along the axis joining the reference star and component c. Olivier & Gavel (1994) derived a formalism to estimate the tilt anisoplanatism for the Keck telescope. Using their estimates and scaling them to the LBT (8.4 m) and wavelength (Ks, $2.15 \mu\text{m}$), we would expect a tilt anisoplanatism of $0''.022$ and $0''.019$ in x and y-direction, respectively. We would thus expect the FWHM of component c to be on the order of $0''.10 - 0''.12$ with an axis ratio of ~ 1.2 . This is much smaller than what we measure. We thus believe that component c is most likely not stellar.

This is in contrast to Quirrenbach et al. (2001) who found component c to be unresolved. Unfortunately, due to the small separation of the two components of the reference star ($0''.135$) and their saturation in the core, they can hardly be used for comparison. A formal Gaussian fit to each of the two components of the reference star ignoring the central saturated pixels (22 pixels

for the brighter and 11 pixels for the fainter component) results in a FWHM of $\sim 0''.08$.

Comp	J	J - H	J - Ks	H - Ks
a	21.81 ± 0.16	1.00 ± 0.19	1.93 ± 0.18	0.93 ± 0.14
b	21.83 ± 0.16	0.93 ± 0.19	1.83 ± 0.18	0.90 ± 0.14
c	22.53 ± 0.13	1.16 ± 0.16	2.07 ± 0.15	0.93 ± 0.11
Total	20.48 ± 0.31	1.05 ± 0.35	2.02 ± 0.34	0.97 ± 0.22

Table 3. JHKs photometry of 3C 294 and its components.

Judging from the images, component c seems to be redder than components a and b. To verify this we performed aperture photometry on the individual components using the apertures indicated in Fig. 3. Calibration was done using star P272–D from Persson et al. (1998); the data have been corrected for galactic extinction following Schlafly & Finkbeiner (2011). It is ≤ 0.01 mag in all bands.

The results shown in Table 3 indicate that components a and b have similar brightnesses and colors, while component c is about 0.7 mag fainter and about 0.2 mag redder. Photometry of the entire system has been presented by McCarthy et al. (1990), Stockton et al. (1999), Quirrenbach et al. (2001), Steinbring et al. (2002), and Toft et al. (2003). A comparison to our data is shown in Table 4. There is a wide spread in the photometry, with differences of up to ~ 1 mag in particular to Toft et al. (2003). It is not clear where the differences in the photometry come from. Unfortunately, the size of the aperture used is not always given.

Photometry of individual components have been derived by Quirrenbach et al. (2001) and Steinbring et al. (2002). A comparison to our data is shown in Table 5. The difference between the Quirrenbach et al. (2001) and Steinbring et al. (2002) data is large, approximately two magnitudes, while our measurements are somewhere in between. Again, the size of the aperture used is not given for either the Keck-data or CFHT-data.

We also created J-H, H-Ks, and J-Ks color maps for 3C 294 to search for any evidence of spatially-dependent extinction in the three components. No obvious feature was detected.

3.2. Optical spectra of the 3C 294 system

The one-dimensional and two-dimensional spectra of the 3C 294 system are shown in Fig. 4. Despite our 2 hr integration time, we do not detect any obvious continuum. When rebinning the spectra in spectral and spatial direction by a factor of five, a hint of continuum can be glimpsed in the red channel. However, with this rebinning, the potential continuum of components a, b, and c would overlap, preventing us from distinguishing between the two components (see below). We detected the Ly α $\lambda 1215 \text{ \AA}$, C IV $\lambda 1550 \text{ \AA}$, He II $\lambda 1640 \text{ \AA}$, and C III] $\lambda 1907/1909 \text{ \AA}$ lines in the blue channel. The C III] line is blue-shifted with respect to the other lines. This is not unusual in AGN (e.g., Barrows et al. (2012)) and may be a result of the increased intensity of the transition at $\lambda 1907 \text{ \AA}$ relative to the one at $\lambda 1909 \text{ \AA}$ at low densities (Ferland 1981).

Only one emission line at $\lambda 6749.4 \text{ \AA}$ can be detected in the red channel. It is faintly present in the individual spectra from both MODS instruments and is not an artifact of the data reduction. Under the assumption that it originates from the same source as the emission lines in the blue channel, we identify this line with the Ne [IV] doublet $\lambda 2424/2426 \text{ \AA}$ at $z = 1.783$. Similarly to our C III] $\lambda 1907/1909 \text{ \AA}$ line in the blue channel we would not be able to separate the double lines individually given

Filter	J	H	K'	Ks	K
LBT	20.48±0.31	19.43±0.17	-	18.56±0.14	-
McCarthy et al. (1990)	-	-	-	-	18.0±0.3
Stockton et al. (1999)	-	-	18.3±0.3	-	-
Quirrenbach et al. (2001)	-	19.4±0.2	18.2±0.2	-	-
Steinbring et al. (2002)	-	18.2±0.3	-	-	17.76±1.0
Toft et al. (2003)	19.53±0.30	18.64±0.27	-	17.78±0.07	-

Table 4. Comparison of JHK photometry of the entire 3C 294 system. To derive the magnitudes from Steinbring et al. (2002), the fluxes from components a, b, and c have been summed.

Filter	H			K		
	a	b	c	a	b	c
LBT	20.88±0.16	20.83±0.11	21.37±0.09	20.04±0.09	19.96±0.09	20.50±0.07
Quirrenbach et al. (2001)	-	-	22.0±0.2	-	-	21.7±0.2
Steinbring et al. (2002)	19.0±0.1	19.5±0.2	20.2±0.2	18.7±0.4	18.4±0.4	19.3±0.8

Table 5. Comparison of HK photometry of components a, b, and c of the 3C 294 system. The K images have been taken through different filters (see Table 4) but the differences are small and did not affect the large differences seen between the individual measurements.

an instrumental resolution of $\sim 5\text{\AA}$. If the identification is correct, we may even associate the very faint emission at $\lambda \sim 6485\text{\AA}$ with C II] $\lambda 2326\text{\AA}$ at $z \sim 1.788$. The position of this line coincides with a forest of night-sky emission lines, however, so this detection is tentative. To our surprise, we do not detect Mg II $\lambda 2798\text{\AA}$ in our spectra, which we would expect at $\lambda \sim 7790\text{\AA}$. However, Mg II is relatively weak in radio galaxies (McCarthy 1993) and line ratios can vary strongly in high-redshift radio galaxies (Humphrey et al. 2008).

Ignoring the redshift determination for the C III] $\lambda 1907/1909\text{\AA}$ line and the uncertain identification of the C II] $\lambda 2326\text{\AA}$ line, our redshift for 3C 294 is $z = 1.784 \pm 0.001$. This is somewhat lower than the redshift $z = 1.786$ quoted by McCarthy et al. (1990), who did not quote errors. With their instrumental resolution of $\sim 12 - 15\text{\AA}$, an error for their redshift δz of at least 0.001 is a fair assumption. Thus our redshifts for 3C 294 agree within the errors. We will use $z = 1.784$ as the redshift for 3C 294 for the remainder of the paper.

Similarly to McCarthy et al. (1990), we see a spatially extended ($6''$) Ly α line. Unfortunately, since the spectra of components a and b overlap in dispersion direction, we cannot probe any dynamics using this line.

The absence of a continuum poses the problem of a unique assignment of the emission line at $\lambda 6749.4\text{\AA}$ to one of the components of 3C 294. To derive this, we did the following: we first fitted a slope through the centers of the emission lines in the blue channel except for the spatially extended Ly α line. We then did the same through the trace in both channels of a well-exposed star observed on the same night to infer the spatial offset. Afterwards we determined the spatial offset between the trace of the star in the blue and the red channels to finally estimate the expected position of the trace of either component in the red channel at $\lambda 6749.4\text{\AA}$. It turned out that the line emission at $\lambda 6749.4\text{\AA}$ is about 4 ± 2 pixels above the expected trace of components a and b and about 3 ± 2 pixels below the expected position of component c. Thus we cannot unambiguously tell whether the line at $\lambda 6749.4\text{\AA}$ originates from the same source as the other UV lines and thus assign it to components a and/or b or c.

4. Discussion

4.1. Which component is associated with the radio source?

There has been no common agreement as to which of the components of the 3C 294 system is indeed the NIR counterpart of the radio source. Using a position of the radio source of $\alpha, \delta = 14^{\text{h}}06^{\text{m}}44^{\text{s}}074 \pm 0^{\text{s}}005, +34^{\circ}25'40''00 \pm 0''05$ (2000) based on McCarthy et al. (1990), Stockton et al. (2004) found it practically coincident with component b. On the contrary, Quirrenbach et al. (2001) associated the radio source with component c. Their positions of the radio core and the reference stars differed by $+0''07$ and $+0''5$ from the ones used by Stockton et al. (2004), respectively. The main difference for the position of the reference star comes from the sources used (HST FGS observation by Stockton et al. (2004) and the USNO–A2.0 catalog by Quirrenbach et al. (2001)). It is surprising that Quirrenbach et al. (2001) associated the radio source with component c although they found a smaller separation between the reference star and the radio source than Stockton et al. (2004). As can be seen from Fig. 2, component b is closer to the reference star than component c.

The most accurate position for the reference star comes from the Gaia Data Release 2 (DR2) (Gaia Collaboration et al. 2016, 2018), which gives $\alpha, \delta = 14^{\text{h}}06^{\text{m}}43^{\text{s}}356, +34^{\circ}11'23''273$ (2000) with an error of about 0.05 mas for α and δ each. The proper motion is $\alpha, \delta = +8.80, 1.66$ mas/yr. Since the spatial resolution of the Gaia DR2 is about $0''.4$, the binary star is not resolved and we can assume that the position given above refers to the center of light. This position is in very good agreement with the one determined by Stockton et al. (2004).

Using the coordinates of the reference star from the Gaia DR2 and the radio coordinates of 3C 294 from Stockton et al. (2004), we can now predict the position of the radio core of 3C 294 on our AO NIR images. We used the crosstalk images of the reference star to predict the position of the center of light of the binary star with an accuracy of ± 1 pixel ($\pm 0''.015$). The result is shown in Fig. 3. As in Stockton et al. (2004), our result indicates that the NIR counterpart to the 3C 294 radio source is component b. The overall error budget (accuracy of center of light for the reference star in our images, errors of the positions for the reference star and the radio source) does not exceed $0''.1$, meaning that component c can be ruled out as the NIR counterpart with high confidence.

4.2. Nature of the NIR counterpart of 3C 294

We are now convinced that (at least) component b is the NIR counterpart to the radio source. We also know that extended redshifted Ly α emission centered on the radio core has been detected (McCarthy et al. 1990). In addition, since our spectroscopic results agree well with McCarthy et al. (1990), the redshift of $z = 1.784$ for 3C 294 is now solid. There is agreement that components a and b show a non-stellar morphology. These components are clearly separated in our H- and Ks-band data. Given our spatial resolution and the distance of 3C 294, we cannot decide whether components a and b represent two galaxies in the process of merging, whether they correspond to a single galaxy with an absorption feature along the line of sight, or whether they are two galaxies at different redshifts.

Surprisingly, both components have similar brightnesses and colors. At $z = 1.784$, our JHKs images correspond roughly to rest-frame BVI-data. With $B-V \sim 1.0$, components a and b seem to be dominated by late stars of type K and M. If we assume that components a and b are galaxies, we obtain $M_K \sim -25.3$ from their Ks-band magnitudes of ~ 20.0 . This includes a lower limit for the K-band correction of $K = -0.5$ (which is between $K = 0$ and -0.5 depending on galaxy type; Poggianti (1997); Mannucci et al. (2001)) at $z = 1.784$. No evolutionary correction has been applied. We note that this is an upper limit for the host galaxy of 3C 294 as we do not know the contribution of the active nucleus to the total flux. If 90/50/10% of the flux from component b is from the host galaxy, we would derive $M_K \sim -25.2/-24.6/-22.8$. This is between 2 mag brighter and 0.4 mag fainter than a M_K^* galaxy (Mortlock et al. 2017).

4.3. Nature of component c

What is the nature of component c? Stockton et al. (2004) discussed the intriguing possibility that 3C 294 hosts two active nuclei. This idea stems from an analysis of archival Chandra data, where the X-ray emission from 3C 294 could better be described by a superposition of two point sources. Based on the X-ray/optical flux ratio, they argued that component c is unlikely to be a foreground galactic star but could well host a second active nucleus. We found component c about 0.8 mag brighter than Quirrenbach et al. (2001), but even then its X-ray/optical flux ratio of ~ 1.1 indicates that the source is rather an AGN than a star using the arguments of Stockton et al. (2004). If it is a star, it could be a carbon star. These stars are often found in symbiotic X-ray binaries (e.g., Hynes et al. (2014)) and have very red V-K and H-K colors similarly to what we found (Ducati et al. 2001). However, with $V-K \sim 5$, and $M_V \sim -2.5$ typical for carbon stars (Alksnis et al. 1998), the distance modulus would place our "star" well outside our Galaxy. In addition, component c appears extended in our data supporting an extragalactic origin.

Unfortunately, the results from our spectroscopy are of little help. We now know that the radio core coincides with component b. It is thus reasonable to assume that the UV lines detected in the blue channel, which have also been seen by McCarthy et al. (1990), originate from that region. We note that (McCarthy et al. 1990) used a 2" wide slit at PA = 200°, which means that their spectra of components a, b, and c overlapped in spectral direction. As discussed in Sect. 3.2, we cannot unambiguously assign the emission line at $\lambda 6749.4 \text{ \AA}$ to component b or c based on its spatial location. Given its spectral position one can reasonably assume that this line originates from the same region as all the other UV lines, namely from component b. If this is the case, the nature of component c remains a mystery.

Although speculative, we briefly discuss the consequences if the emission line at $\lambda 6749.4 \text{ \AA}$ belongs to component c. One exciting alternative would be that the line originates from the Ne [IV] doublet $\lambda 2424/2426 \text{ \AA}$ at $z = 1.783$ from this component. This would make 3C 294 indeed a dual, perhaps bound AGN separated by a few kiloparsec as discussed by Stockton et al. (2004). However, they speculated that the AGN coincident with component c is less powerful but does not suffer so much from extinction. In that case one would expect to see the UV lines (in particular Ly α , which is typically a factor of ~ 60 stronger than Ne [IV] $\lambda 2424/2426 \text{ \AA}$ in radio galaxies (McCarthy 1993)) in the blue channel, unless they are unusually weak. An inspection of the two-dimensional spectrum in the blue channel did not reveal any second component in spatial direction. Thus we do not have strong support for the dual AGN scenario based on our spectroscopy.

If not at the same redshift, component c could be at a different redshift. Given the faintness of the optical counterpart and emission line, and showing X-ray emission, it most likely originates from an AGN. Judging from the composite AGN spectrum of Vanden Berk et al. (2001), the most prominent lines in the optical are H α , H β , the [O II], [O III] lines, and Mg II. Out of these, it cannot be H α at $z = 0.029$, because its NIR luminosity would be much too low unless it suffers from extreme absorption. It also cannot be H β at $z = 0.38$ because then we should have seen H α at $\lambda 9054 \text{ \AA}$, which is normally much stronger, and/or the [O II] or [O III] lines at $\lambda 3727$ and $\lambda 5007 \text{ \AA}$, respectively. The same argument applies for the [O III] line at $z = 0.35$. The [O II] line at $z = 0.81$ would be an interesting possibility. The typically much stronger H β and [O III] lines would be shifted towards $\lambda 9000 \text{ \AA}$, where there is a strong forest of night-sky emission lines. However, one would then easily see Mg II $\lambda 2798 \text{ \AA}$, which is normally also stronger than [O II]. Thus, Mg II $\lambda 2798 \text{ \AA}$, which would be at $z = 1.41$, remains as the most reasonable line identification. All optical emission lines redward of Mg II are redshifted beyond $\lambda 9000 \text{ \AA}$ and are thus hard to detect or are out of the optical range. Only the C IV and C III] UV lines remain. These would be redshifted to $\lambda 3735$ and $\lambda 4600 \text{ \AA}$, respectively, but are not present in our spectra. These lines are often faint or not present in type II quasi stellar object (QSO) candidates at high redshift (Alexandroff et al. 2013), so it would not be surprising. One caveat of all of the options discussed above is that even at $z = 1.41$ the host galaxy of an AGN must substantially absorb the emission from 3C 294. This has not been seen. Thus, even the most reasonable option (Mg II at $z = 1.41$) is not convincing.

Alternatively, the emission line in component c could derive from a redshifted UV line. The strongest UV lines in a QSO spectrum are Ly α $\lambda 1215 \text{ \AA}$, C IV $\lambda 1549 \text{ \AA}$, and C III] $\lambda 1909 \text{ \AA}$ (Vanden Berk et al. 2001). This would move the AGN to redshifts beyond $z = 2.5$, with 3C 294 then being along the line of sight to component c. Its redshift would then be $z = 2.54$ (C III]), 3.36 (C IV), or 4.56 (Ly α), respectively. If this is the case, the UV lines should be absorbed to some extent by 3C 294.

There are eight QSO at $z > 2.5$, up to $z = 5.2$, in the Chandra Deep Field North (CDFN, Brandt et al. (2001); Barger et al. (2002)). These eight sources all share the same properties with component c. Their soft X-ray flux in the 0.5-2.0 keV band is between 0.3 and $6 \times 10^{-15} \text{ ergs cm}^{-2} \text{ s}^{-1}$, their K magnitudes are ~ 21 , their V magnitudes are ~ 24 , and their spectroscopic signatures include strong, broad Ly α , sometimes also accompanied by strong C+IV and C III]. Given the faintness of our emission

line and the absence of a second line, it is reasonable to assume that this would correspond to Ly α at $z = 4.56$.

4.4. Consequences for an AGN pair

Our results do not allow us to discriminate between the dual AGN or projected AGN scenario. Even the latter would not contradict the interpretation by Stockton et al. (2004) that 3C 294 hosts an obscured AGN centered at component b, while a second much fainter but not obscured AGN is coincident with component c. One natural explanation for the differences in the photometry from various studies summarized in Table 4 is the intrinsic variability of the two AGN.

Projected AGN pairs can be used for a number of astrophysical applications. Examples are QSO-QSO clustering and the tomography of the intergalactic medium or the circumgalactic medium of the QSO along the light of sight to the background QSO (Hennawi et al. 2006). The latest compilation of projected QSO pairs can be found in Findlay et al. (2018). However, the number of small-separation pairs (a few arcsec) is very small (Inada et al. 2012; More et al. 2016), and they have mostly been derived from searches for gravitationally lensed QSOs and all have a wider separation ($\geq 2''$) than our target. To the best of our knowledge, no projected AGN pair with such a small separation and large Δz is known at present.

Due to the close separation of our system, gravitational lensing effects could modify the apparent properties of the 3C 294 system. A multiply-lensed QSO image of component c would be expected for an Einstein radius of $\geq 1''$. Since we do not see any, this would set the upper limit of the 3C 294 host galaxy to $3 \times 10^{12} M_{\odot}$ at a redshift of $z = 1.784$ and 4.56 for the lense and source, respectively. As the host galaxy is certainly not point-like, any amplification must be very low. In addition, component c could even be subject to gravitational microlensing by stars in the host galaxy of 3C 294. This might at least in part explain the difference in brightness of the 3C 294 system shown in Table 4.

4.5. Outlook

The analysis of our deep AO images and optical spectra of 3C 294 did not allow us to unambiguously characterize the 3C 294 system as the main conclusion rests on the spatial association of the emission line at $\lambda 6749.4 \text{ \AA}$ with either component b or c. If it originates from component b, the nature of component c remains a mystery. If it originates from component c, we have support for either the dual or projected AGN scenario. Whether the lines originate from component b or c can be tested by repeating the optical spectroscopy "astrometrically" by taking a spectrum of 3C 294 and a bright object on the FoV simultaneously, with the latter showing a trace on the two-dimensional spectrum. If the line at $\lambda 6749.4 \text{ \AA}$ belongs indeed to component c, AO-aided NIR spectroscopy is the only way to characterize the system due to the faintness of the system and the probably high redshifts involved. Not much can be learned for 3C 294 itself from the ground, as at $z = 1.784$ all diagnostic optical emission lines except H_{γ} will be redshifted into a wavelength range where the NIR sky is opaque. At least one of the redshifted [O II, O III] or $H\alpha, \beta$ lines is redshifted into one of the JHK-windows if component c is at $z = 2.54, 3.36, \text{ or } 4.56$. An unambiguous determination of the nature of 3C 294 will be possible with the NIR spectrograph NIRspec onboard the James Webb Space Telescope. With its $3'' \times 3''$ Integral Field Unit covering the wavelength range $0.67 - 5 \mu\text{m}$, a number of diagnostic

lines can be observed in a very low infrared background devoid of opaque wavelength regions.

Acknowledgements. We would like to thank the anonymous referee for the constructive comments that addressed a number of important points in the paper. We would also like to thank Mark Norris and Jesper Storm for taking the MODS-data at the LBT for us. This work has made use of data from the European Space Agency (ESA) mission *Gaia* (<https://www.cosmos.esa.int/gaia>), processed by the *Gaia* Data Processing and Analysis Consortium (DPAC, <https://www.cosmos.esa.int/web/gaia/dpac/consortium>). Funding for the DPAC has been provided by national institutions, in particular the institutions participating in the *Gaia* Multilateral Agreement. This work was supported in part by the German federal department for education and research (BMBF) under the project numbers 05 AL2VO1/8, 05 AL2EIB/4, 05 AL2EEA/1, 05 AL2PCA/5, 05 AL5VH1/5, 05 AL5PC1/1, and 05 A08VH1.

References

- Alexandroff, R., Strauss, M. A., Greene, J. E., et al. 2013, MNRAS, 435, 3306
 Alksnis, A., Balklavs, A., Dzervitis, U., & Egļitis, I. 1998, A&A, 338, 209
 Barger, A. J., Cowie, L. L., Brandt, W. N., et al. 2002, AJ, 124, 1839
 Barrows, R. S., Stern, D., Madsen, K., et al. 2012, ApJ, 744, 7
 Brandt, W. N., Alexander, D. M., Hornschemeier, A. E., et al. 2001, AJ, 122, 2810
 Ducati, J. R., Bevilacqua, C. M., Rembold, S. B., & Ribeiro, D. 2001, ApJ, 558, 309
 Esposito, S., Riccardi, A., Pinna, E., et al. 2012, in Proc. SPIE, Vol. 8447, Adaptive Optics Systems III, 84470U
 Fabian, A. C., Sanders, J. S., Crawford, C. S., & Etorri, S. 2003, MNRAS, 341, 729
 Ferland, G. J. 1981, ApJ, 249, 17
 Findlay, J. R., Prochaska, J. X., Hennawi, J. F., et al. 2018, ApJS, 236, 44
 Gaia Collaboration, Brown, A. G. A., Vallenari, A., et al. 2018, A&A, 616, A1
 Gaia Collaboration, Prusti, T., de Bruijne, J. H. J., et al. 2016, A&A, 595, A1
 Heidt, J., Pramskiy, A., Thompson, D., et al. 2018, in Society of Photo-Optical Instrumentation Engineers (SPIE) Conference Series, Vol. 10702, Ground-based and Airborne Instrumentation for Astronomy VII, 107020B
 Hennawi, J. F., Prochaska, J. X., Burles, S., et al. 2006, ApJ, 651, 61
 Humphrey, A., Villar-Martín, M., Vernet, J., et al. 2008, MNRAS, 383, 11
 Husemann, B., Worseck, G., Arrigoni Battaia, F., & Shanks, T. 2018, A&A, 610, L7
 Hynes, R. I., Torres, M. A. P., Heinke, C. O., et al. 2014, ApJ, 780, 11
 Inada, N., Oguri, M., Shin, M.-S., et al. 2012, AJ, 143, 119
 Kormendy, J. & Ho, L. C. 2013, ARA&A, 51, 511
 Koss, M., Mushotzky, R., Treister, E., et al. 2012, ApJ, 746, L22
 Mannucci, F., Basile, F., Poggianti, B. M., et al. 2001, MNRAS, 326, 745
 McCarthy, P. J. 1993, ARA&A, 31, 639
 McCarthy, P. J., Spinrad, H., van Breugel, W., et al. 1990, ApJ, 365, 487
 Miley, G. & De Breuck, C. 2008, A&A Rev., 15, 67
 Monet, D. 1998, USNO-A2.0
 More, A., Oguri, M., Kayo, I., et al. 2016, MNRAS, 456, 1595
 Mortlock, A., McLure, R. J., Bowler, R. A. A., et al. 2017, MNRAS, 465, 672
 Olivier, S. S. & Gavel, D. T. 1994, Journal of the Optical Society of America A, 11, 368
 Overzier, R. A., Shu, X., Zheng, W., et al. 2009, ApJ, 704, 548
 Persson, S. E., Murphy, D. C., Krzemiński, W., Roth, M., & Rieke, M. J. 1998, AJ, 116, 2475
 Pogge, R. 2019, rwpogge/modsCCDRed 2.0, modsCCDRed was developed for the MODS1 and MODS2 instruments at the Large Binocular Telescope Observatory, which were built with major support provided by grants from the U.S. National Science Foundation's Division of Astronomical Sciences Advanced Technologies and Instrumentation (AST-9987045), the NSF/NOAO TSIP Program, and matching funds provided by the Ohio State University Office of Research and the Ohio Board of Regents. Additional support for modsCCDRed was provided by NSF Grant AST-1108693.
 Pogge, R. W., Atwood, B., Brewer, D. F., et al. 2010, in Proc. SPIE, Vol. 7735, Ground-based and Airborne Instrumentation for Astronomy III, 77350A
 Poggianti, B. M. 1997, A&AS, 122, 399
 Quirrenbach, A., Roberts, J. E., Fidkowski, K., de Vries, W., & van Breugel, W. 2001, ApJ, 556, 108
 Rosas-Guevara, Y. M., Bower, R. G., McAlpine, S., Bonoli, S., & Tissera, P. B. 2019, MNRAS, 483, 2712
 Rothberg, B., Kuhn, O., Power, J., et al. 2018, in Society of Photo-Optical Instrumentation Engineers (SPIE) Conference Series, Vol. 10702, Ground-based and Airborne Instrumentation for Astronomy VII, 1070205
 Saxena, A., Marinello, M., Overzier, R. A., et al. 2018, MNRAS, 480, 2733
 Schlafly, E. F. & Finkbeiner, D. P. 2011, ApJ, 737, 103
 Steinbring, E., Crampton, D., & Hutchings, J. B. 2002, ApJ, 569, 611
 Stockton, A., Canalizo, G., Nelan, E. P., & Ridgway, S. E. 2004, Astrophysical Journal, 600, 626
 Stockton, A., Canalizo, G., & Ridgway, S. E. 1999, ApJ, 519, L131
 Toft, S., Pedersen, K., Ebeling, H., & Hjorth, J. 2003, MNRAS, 341, L55
 Urry, C. M. & Padovani, P. 1995, PASP, 107, 803
 Vanden Berk, D. E., Richards, G. T., Bauer, A., et al. 2001, AJ, 122, 549

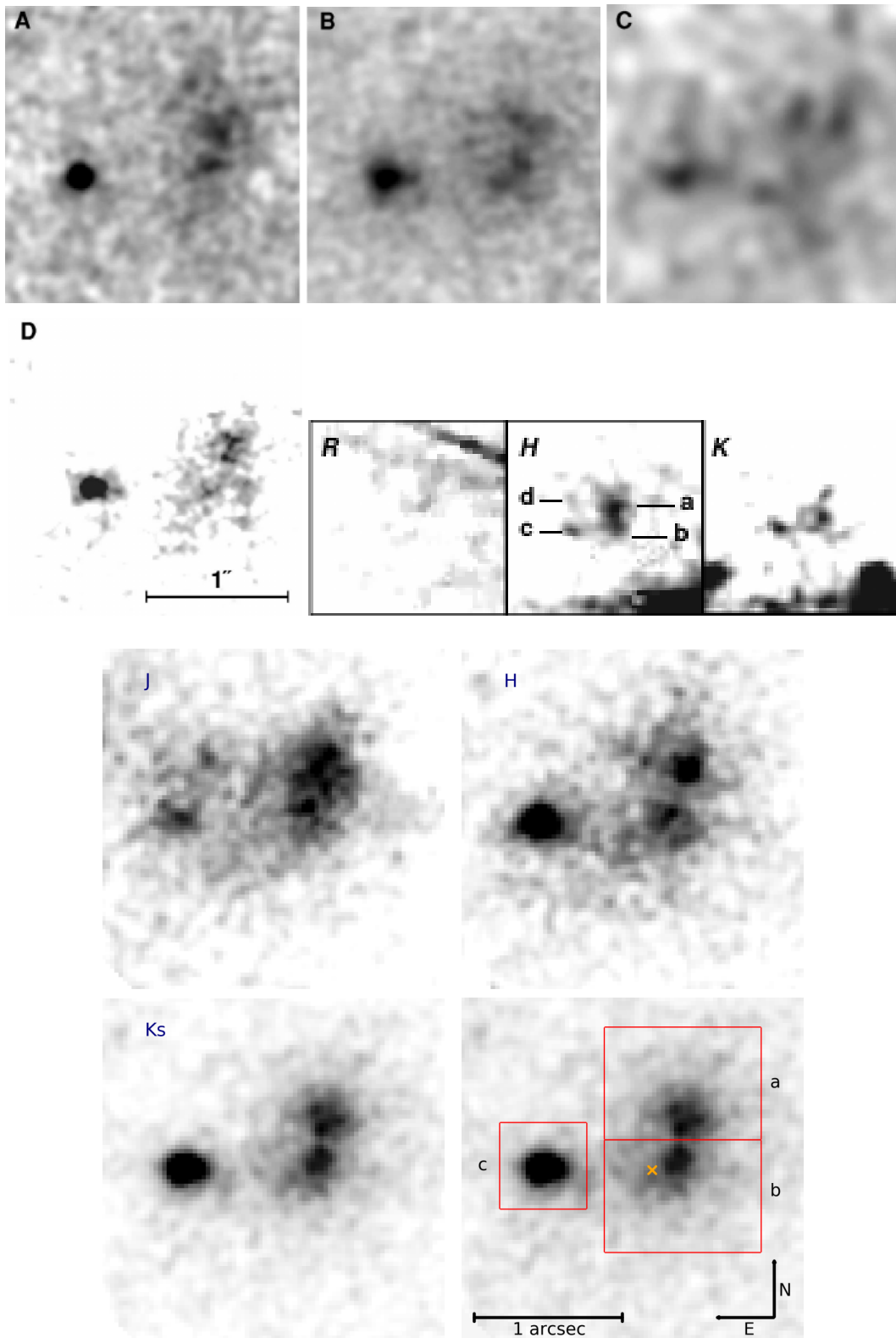


Fig. 3. Two uppermost rows) AO NIR images of 3C 294 from earlier publications. A) Keck II NIRSPEC K' image from Stockton et al. (2004), B) Subaru IRCS K' image also from Stockton et al. (2004), C) CFHT Hokupa K' image from Stockton et al. (1999), and D) Keck II SCam H-band image from Quirrenbach et al. (2001). The images A-D are adapted from Stockton et al. (2004). The three images right of image D show R (HST), H, and K CFHT PUEO data from Steinbring et al. (2002). Two lowest rows) Our LBT FLAO and LUCI JHKs-images of 3C 294. The fourth image shows the scale, orientation, and apertures for the components used for the photometric analysis. They are 36×26 pixel ($0''.54 \times 0''.39$) for components a and b and 20×20 pixel ($0''.3 \times 0''.3$) for component c. The labeling follows Steinbring et al. (2002). The cross marks the position of the radio core, its size reflects its positional error.

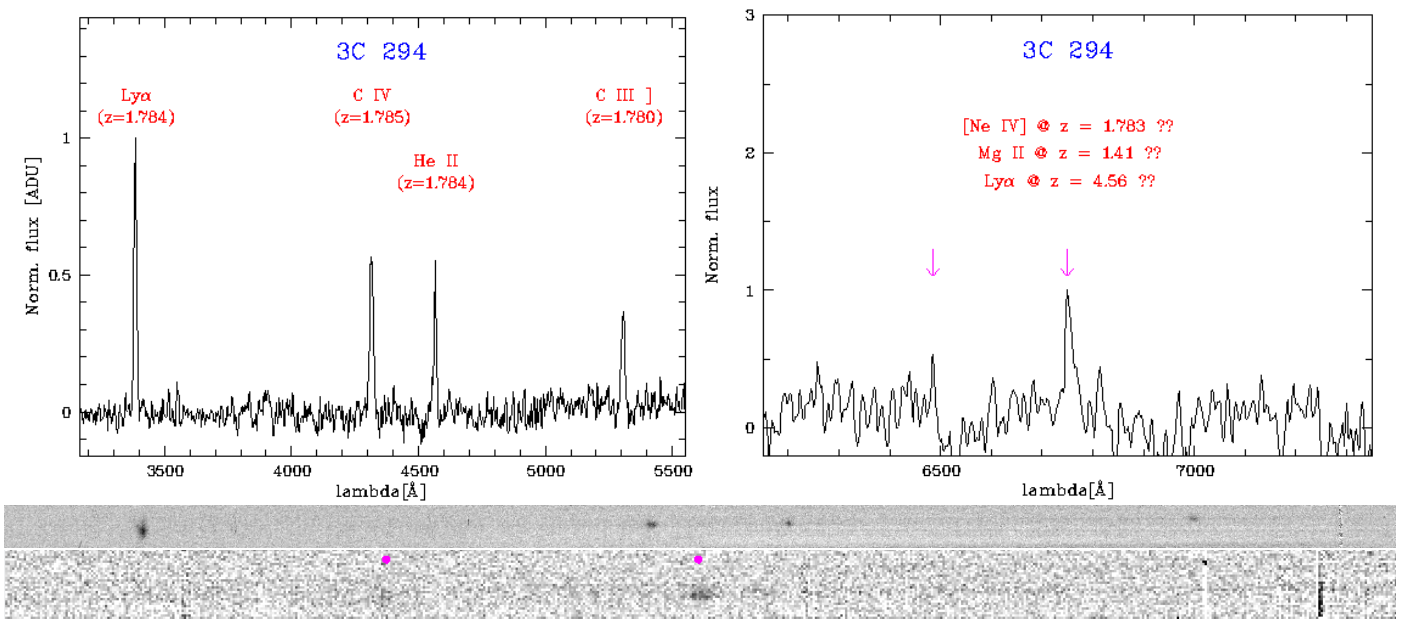


Fig. 4. Top) Our one-dimensional MODS spectra of the 3C 294 system in the blue (left) and (red) channel with the line identifications. The positions of the two emission features at $\lambda 6485$ and $\lambda 6749.4$ Å discussed in the text are indicated by arrows. Bottom) Our two-dimensional MODS spectrum of the 3C 294 system in the blue channel (upper panel) showing the four emission lines as well as an excerpt of the two-dimensional spectrum in the red channel (lower panel) showing the emission line detected at $\lambda 6749.4$ Å. The blue spectrum is shown across its full spectral range, the red spectrum with an identical width then the one-dimensional spectrum centered on the line at $\lambda 6749.4$ Å. The two emission features are labeled by magenta dots.